

Triboelectric Nanogenerator Accelerates Highly Efficient Nonviral Direct Conversion and In Vivo Reprogramming of Fibroblasts to Functional Neuronal Cells

Yoonhee Jin, Jungmok Seo, Jung Seung Lee, Sera Shin, Hyun-Ji Park, Sungjin Min, Eunji Cheong, Taeyoon Lee,* and Seung-Woo Cho*

COMMUNICATION

Direct conversion is an efficient strategy to produce effective cell therapeutics for treating neuronal disorders without using stem or progenitor cells. Several studies have attempted to obtain neuronal cells by differentiating adult, embryonic, or reprogrammed stem cells but have encountered significant inherent limitations associated with stem cells. Recent studies have shown that delivery of gene sets encoding cell lineage-specific transcription factors (TFs) directly reprograms somatic cells into cells of other lineages without inducing their transition through pluripotent stem cell-like state.^[1] Thus, the direct cell conversion strategy avoids ethical issues associated with the use of human embryos and reduces the risk of tumorigenesis associated with the use of pluripotent stem cells. Because of these therapeutic advantages, direct reprogramming to obtain neuronal or glial lineage cells has been extensively studied after the identification of novel reprogramming factors (e.g., TFs and microRNAs^[2]) that generate neuronal subtype lineages, including dopaminergic,^[3] cholinergic,^[4] and motor neurons,^[5] and glial lineage cells, including oligodendrocytes^[6] and astrocytes.^[7]

However, one of the major obstacles in the clinical application of this technology is the use of viral vectors for delivering genes encoding reprogramming factors. Viral vectors are widely used to deliver exogenous genes for direct conversion of somatic cells because of their high efficacy; however, safety issues due to the immunogenicity and tumorigenicity of these vectors restrict their clinical application.^[8] Therefore, a novel direct conversion platform involving nonviral gene delivery is urgently required to accelerate the generation of induced neuronal (iN) cells, with

minimal safety issues, in clinical settings.^[8d] A study reported nonviral polymer nanoparticle-mediated direct conversion of mouse fibroblasts to iN cells; however, conversion efficiency of this strategy was low. This suggests the need for external stimulation to compensate for the low efficiency of nonviral vectors and to facilitate neuronal lineage conversion.

Electrical stimulation can be considered for enhancing the direct conversion of fibroblasts to neuronal cells. Several studies have reported important roles of naturally occurring endogenous electrical cues associated with tissue morphogenesis during development, especially neuronal cell differentiation and maturation. Studies have shown that electrical stimulation promotes the growth,^[9] differentiation,^[10] and axonal regeneration^[11] of neurons and stem cells. These findings suggest that electrical stimulation during nonviral direct conversion facilitates the transdifferentiation of fibroblasts to iN cells.

In this study, we applied triboelectrification as an electrical stimulation source to generate periodic biphasic pulse-like currents for direction conversion to produce iN cells. Energy harvesting from mechanical energy such as vibrational motion and mechanical deformation has attracted great attention because it serves as a sustainable electrical power source for various micro- and nanosystems.^[12] Recent studies have regarded a novel mechanical energy-harvesting device, triboelectric nanogenerator,^[13] as one of the most promising candidates for developing implantable electronics such as self-powered pacemakers^[14] because it generates electricity from human motion in a simple, cost-effective manner. Thus, unique periodic pulse-like electrical signals generated from a triboelectric generator that mimic naturally occurring currents in the body can be used for electrical stimulation during direct cell reprogramming. Recently, Tang et al. highlighted the potential biological application of triboelectricity that a triboelectric-powered low-level laser cure system enhanced osteogenesis.^[15]

Here, we established a biphasic triboelectrical stimulation platform to achieve highly efficient nonviral direct conversion of primary mouse embryonic fibroblasts (PMEFs) to iN cells. Genes encoding neuronal lineage-specific TFs Brn2, Ascl1, and Myt1l (BAM TFs) were delivered into PMEFs through electroporation and by using biodegradable polymeric nanoparticles. During cell conversion, highly conductive titanium (Ti)-deposited silicon (Si) connected to a triboelectrical stimulator (TES), which generated biphasic electrical signals (open-circuit voltage [V_{oc}], ≈ 30 V; short-circuit current [I_{sc}], ≈ 270 nA), was used as a cell culture substrate. The stimulated PMEFs

Dr. Y. Jin, J. S. Lee, H.-J. Park, S. Min, Prof. E. Cheong,
Prof. S.-W. Cho

Department of Biotechnology
Yonsei University

50 Yonsei-ro, Seodaemun-gu
Seoul 120-749, Republic of Korea
E-mail: seungwoocho@yonsei.ac.kr

Dr. J. Seo, S. Shin, Prof. T. Lee
School of Electrical and Electronic Engineering
Yonsei University

50 Yonsei-ro, Seodaemun-gu, Seoul 120-749, Republic of Korea
E-mail: taeyoon.lee@yonsei.ac.kr

Prof. S.-W. Cho
Department of Neurosurgery
Yonsei University College of Medicine
Seoul 120-750, Republic of Korea

DOI: 10.1002/adma.201601900



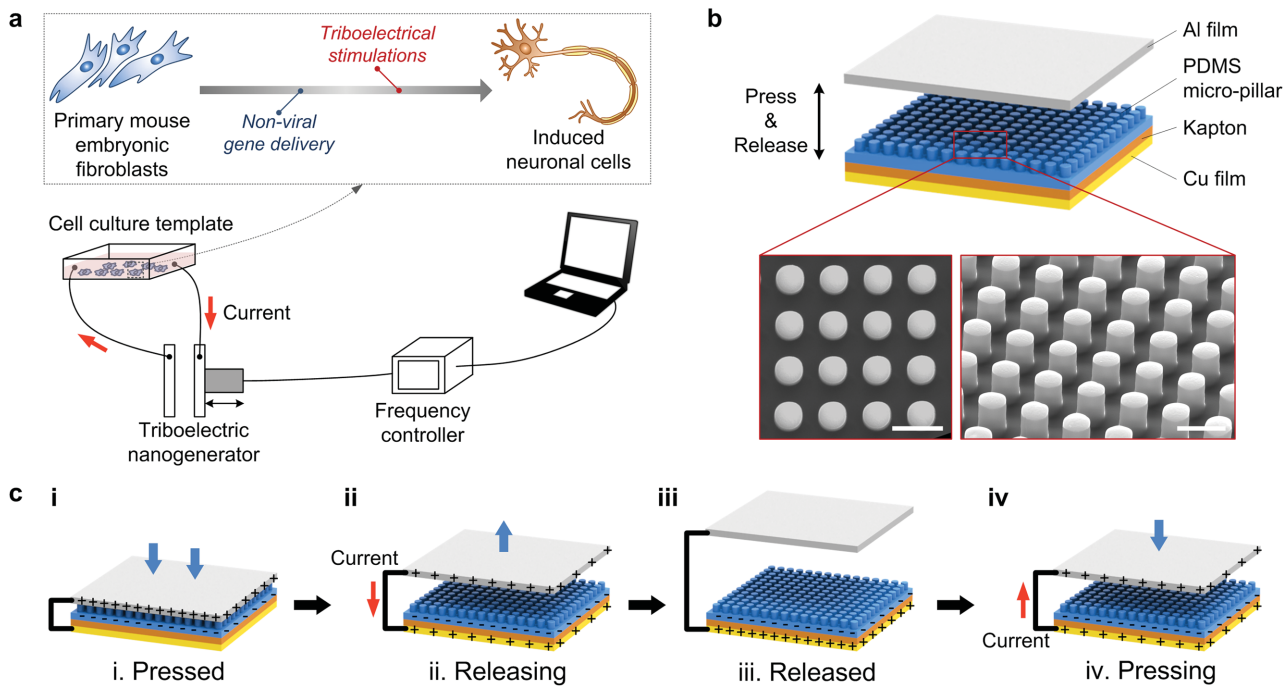


Figure 1. Experimental set-up of TES for the nonviral direct conversion of PMEFs to iN cells. a) Schematic representation of the experimental set-up of TES for efficient direct cell conversion. b) Structural design and SEM images of TES (scale bars = 5 μm). c) A cycle of electricity generation for illustrating the operating principle of TES.

underwent accelerated transdifferentiation at high efficiency to produce iN cells with mature phenotypes and improved electrophysiological functionalities. Furthermore, use of the TES greatly enhanced *in vivo* iN cell generation in the skin tissues of mice. These results suggest that use of the TES and polymer nanoparticles for direct cell conversion can efficiently generate functional neuronal cells for cell replacement therapy of neurodegenerative diseases.

TES was connected in series with the highly conductive Ti-coated cell culture substrate to achieve efficient direct conversion of PMEFs to iN cells (Figure 1a). Direct cell conversion was facilitated by applying biphasic electrical stimulation after nonviral delivery of genes encoding BAM TFs. TES generates biphasic pulse-type electrical signals based on contact electrification between its top and bottom plates. Pulse frequency of TES can be controlled using a computer-based interface. Schematic representation of the structure of TES is shown in Figure 1b. Because electricity generation by TES is based on contact electrification, we chose plates made of aluminium (Al) and polydimethylsiloxane (PDMS) as the top and bottom plates, respectively, which were located at the two ends of triboelectric series. For preparing the bottom plate, a micro-pillar-structured PDMS layer (thickness, $\approx 300 \mu\text{m}$) was glued to a Kapton film. Next, the Kapton film with the structured PDMS layer was attached to a copper (Cu) electrode. Morphology of the structured PDMS layer was characterized using a scanning electron microscope (SEM) to confirm that the pillar arrays were uniform and regular across a large area (Figure 1b). The micro-pillar-structured PDMS was used to enhance triboelectric charging.^[16] Another TES was fabricated in the same manner

by using a flat PDMS film of the same thickness to compare the generated electricity.

Electrical stimulation by TES is based on the periodic press and release of the top and bottom plates that are parallel to each other. Figure 1c schematically illustrates the operating principle of TES. In the initial state, when the top and bottom plates are separated, no electrical potential difference is observed because of the absence of contact-induced charge transfer. Contact between the top and bottom plates induces surface friction, which results in electron transfer from the Al layer to the PDMS layer. The surfaces of the Al and PDMS layers are positively and negatively charged, respectively (Figure 1c-i). In the pressed state, the TES is in electrostatic equilibrium because the generated triboelectric charges stay on the contacted surfaces. In the releasing state, negative triboelectric charges on the PDMS layer are retained because of the insulating nature of this plate and opposite charges are produced on the surfaces of the Cu electrode and Kapton film. This produces electrical potential difference between the 2 plates and induces the movement of electrons from the bottom electrode to the top electrode through an external load to compensate the charge difference (Figure 1c-ii). The flow of electrons continues until a sufficient distance is achieved between the top and bottom plates, after which the TES achieves electrostatic equilibrium (Figure 1c-iii). Once the top plate is pressed again, electrons flow from the top electrode to the bottom electrode through the external load with opposite direction of current flow compared to the releasing process (Figure 1c-iv). Therefore, the TES can serve as a self-powered electrical stimulator that generates biphasic electricity for efficient direct cell conversion.

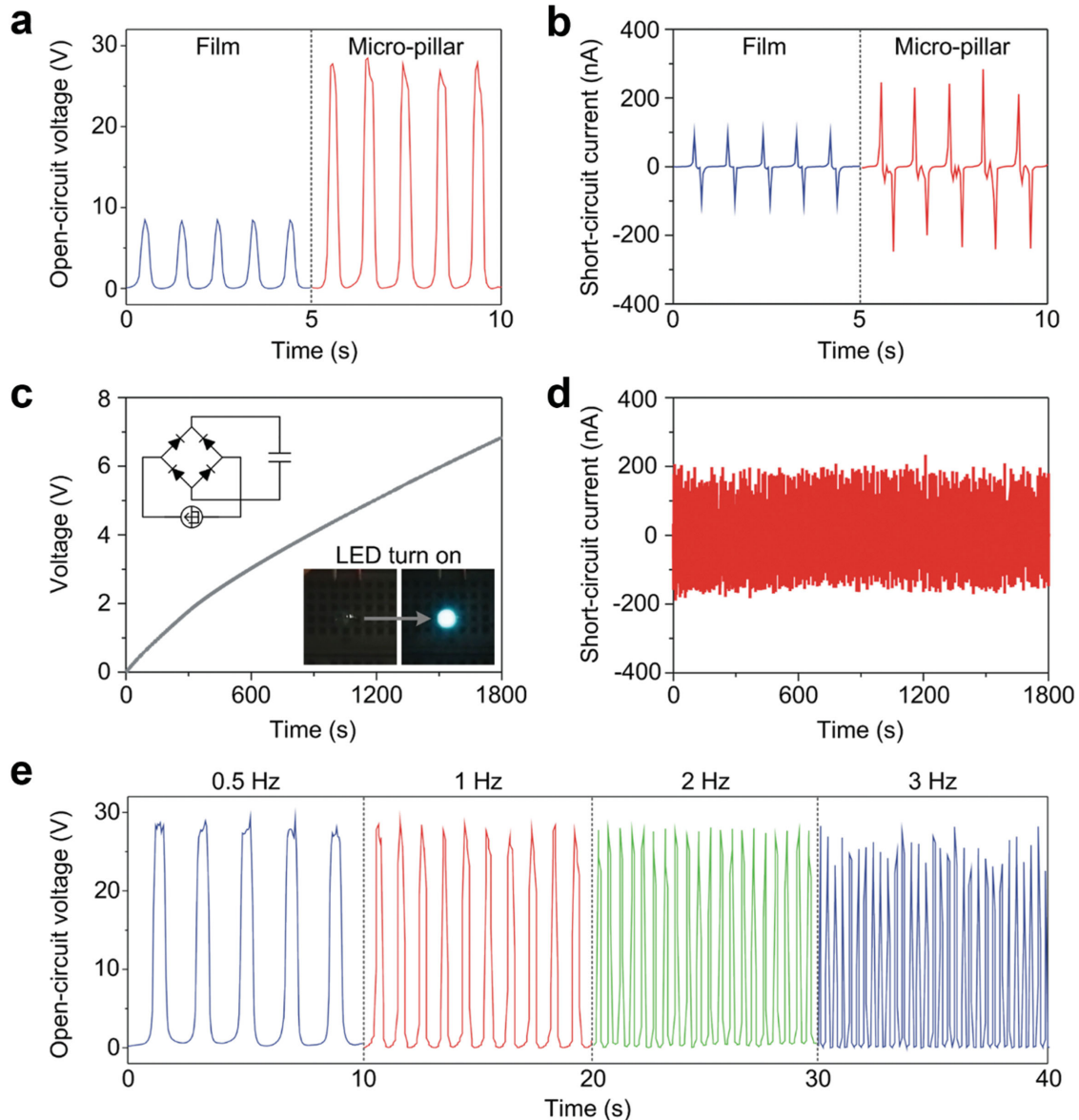


Figure 2. Electrical output performances of TES. a) Output open-circuit voltage of TES with flat and micro-pillar-structured PDMS layers at 1 Hz pulse frequency. b) Short-circuit current of TES at 1 Hz pulse frequency. c) Charging curve of the capacitor obtained using rectified electricity generated by TES. Left inset shows a schematic circuit diagram of the electric rectifier and capacitor. A commercial blue LED bulb lightened up by the charged capacitor (right inset). d) Results of the stability test of TES at 1 Hz pulse frequency. e) Effect of contact frequencies (0.5, 1, 2, and 3 Hz) between the top and bottom electrodes on the open-circuit voltage.

TES produces controllable, naturally occurring electrical cues to facilitate direct cell conversion. Figure 2a,b shows TES-generated V_{oc} and I_{sc} , respectively, under periodic contact, with 1-Hz frequency. TES successfully generates biphasic current pulses by converting mechanical energy of periodic contact. To investigate the structural effect of the PDMS layer on the output performance of TES, we compared electrical characterization of TES devices with flat and micro-pillar-structured PDMS layers. Output voltage and current from TES with the micro-pillar-structured PDMS layer were much higher ($V_{oc} \approx 30$ V; $I_{sc} \approx 280$ nA) than those from TES with the flat PDMS layer ($V_{oc} \approx 10$ V; $I_{sc} \approx 110$ nA) under the same condition

of mechanical contact. Therefore, TES with the micro-pillar-structured PDMS layer was used to accelerate direct cell conversion. Electricity generated by TES at 1 Hz contact frequency was stored in a 22 μ F capacitor, which was connected to a full-wave rectifying bridge (Figure 2c). The voltage of the capacitor was gradually increased under the continuous contact process and the charged capacitor could light up a commercial blue light emitting diode (LED; lower-right inset of Figure 2c). Cycling stability test was performed to confirm the mechanical robustness and durability of the TES. During the cycling contact between top and bottom plates, there was no noticeable degradation of biphasic electrical output of the TES (Figure 2d).

Figure 2e shows the output voltages of the TES at varying contact frequencies (0.5–3 Hz) between the top and bottom plates. Our results indicated that the TES was stable under various mechanical contact conditions.

TES was used to facilitate the direct conversion of PMEFs to iN cells after nonviral delivery of genes encoding BAM TFs through electroporation and polymer nanoparticle-mediated transfection. The experimental scheme for generating iN cells is described in Figure 3a. PMEFs were transfected with BAM TF-expressing plasmids through electroporation (2.4 µg plasmids per 10^5 cells) and were seeded onto poly-L-lysine-/laminin-coated Ti/Si substrates. Two days after the seeding, the cells were transfected again with the BAM TF-expressing plasmids by using C32-122 poly(β-amino ester) (PBAE) nanoparticles (3.0 µg plasmids per 10^5 cells). PBAE nanoparticles are cationic polymers that self-assemble with DNA to form nanoparticles with a diameter of 100–150 nm. We previously reported that these nanoparticles showed effective transfection efficiencies, with relatively low cytotoxicities, in various cells.^[17] Amine end-modified PBAE nanoparticles, including C32-122 PBAE nanoparticles, show high transfection efficiency, particularly in primary cells, even in the presence of serum.^[17a,b] Cell culture medium was replaced with neuronal induction medium on the day after the second transfection (3 d after the cell seeding), and the cells were exposed to the TES (frequency, 1 Hz) every day for 60 min per day (Figure 3a). Efficiency of iN cell generation was determined by staining the cells for neuronal marker class III beta-tubulin (Tuj1) on days 9 and 12–14.

TES-generated biphasic electrical cues significantly enhanced the efficiency of nonviral direct conversion of PMEFs to iN cells and accelerated the conversion rate. Transfection of PMEFs with BAM TF-expressing plasmids and their subsequent maintenance in neuronal induction medium and exposure to TES (BAM/TES group) produced iN cells with an elongated neuronal-like morphology on day 9, of which many cells were Tuj1 positive (Figure 3b). PMEFs transfected with BAM TF-expressing plasmids but not exposed to TES (BAM group) produced less number of Tuj1-positive cells on day 9. On day 12 after the transfection, Tuj1-positive cells were observed in both the BAM/TES and BAM groups (Figure S1, Supporting Information). In contrast, PMEFs not transfected with BAM TF-expressing plasmids but exposed to TES (TES group) and PMEFs not transfected with BAM TF-expressing plasmids and not exposed to TES (NT group) but otherwise treated identically did not show any morphological changes and produced only a few Tuj1-positive cells (Figure S1, Supporting Information). On day 9, the conversion efficiency, which was calculated as a percentage ratio of Tuj1-positive cells to the total number of cells seeded, of cells in the BAM group was 0.13% (Figure 3c). Whereas, the obtained conversion efficiency of cells in the BAM/TES group was 8.85% (Figure 3c). On days 12–14, the conversion efficiency of cells in the BAM group increased to 6.41% and that of cells in the BAM/TES group increased to 14.17% (Figure 3c). These results suggested that exposure of cells to TES after the nonviral delivery of genes encoding conversion factors substantially accelerated the transdifferentiation of fibroblasts to neuronal cells.

Increased expression of neuronal lineage-related markers such as nestin, Tuj1, and microtubule associated protein

2 (MAP2) in PMEF-derived reprogrammed cells on days 6 and 12 was verified by performing quantitative reverse transcription-polymerase chain reaction (qRT-PCR) (Figure 3d,e). Cells in the BAM/TES group showed the highest expression levels of the 3 makers at both the time points. Effect of TES exposure on reprogrammed cells was more evident on day 12, as confirmed by the 1.5–2-fold increase in the expression of Tuj1 and MAP2, compared with that in cells in the BAM group not exposed to TES (Figure 3e). This finding suggested that TES facilitated the conversion of PMEFs to iN cells by inducing higher expression of neuronal-related genes. Noticeably, cells in the TES group, which were not transfected with BAM TF-expressing plasmids, showed increased expression of early neuronal marker nestin on day 6 and of Tuj1 on day 12 (Figure 3d,e). However, upregulated expression of nestin and Tuj1 was insufficient for producing iN cells with neuronal-like morphology, as evidenced by the negligible number of Tuj1-positive cells (0.22%) found in this group (Figure 3c). In addition, we confirmed that nonviral gene delivery with TES induced the conversion of postnatal cells, tail-tip fibroblasts, to Tuj1 and MAP2 co-positive iN cells (Figure S2, Supporting Information).

To examine the effect of the TES output on neuronal transdifferentiation to generate iN cells from PMEFs, we have compared neural-specific gene expression levels of BAM factor-transfected PMEFs maintained for 7 d under TES with different short-circuit currents. BAM-transfected cells were exposed to 1 Hz TES with a magnitude of \approx 110 and 280 nA generated by flat and micro-pillar-structured PDMS films, respectively. It was observed that the gene expression of neuronal markers Tuj1 and MAP2 was much higher in cells treated with 280 nA TES than in cells treated with 110 nA (Figure S3, Supporting Information). Similar observation was previously reported by Chang et al. demonstrating that biphasic electrical current stimulation promoted proliferation and neuronal differentiation of fetal neural stem cells in an intensity-dependent manner.^[18] Based on our result and previous literature, it is thought that the intensity of electrical stimulation generated by TES likely affects iN conversion efficiency and rate as well as neuronal transdifferentiation.

TES exposure facilitated the neuronal maturation of iN cells. Majority of iN cells exposed to TES showed an elaborate neuronal morphology by days 14–18. After 14 d of culture, cells in the BAM/TES group showed distinct neuronal morphology, with highly elongated neurites (Figure 3f). Some of these cells yielded positive results for neuronal-specific cytoskeletal protein MAP2. However, none of the cells in the BAM group yielded positive results for MAP2 on day 14, suggesting that TES exposure accelerated the neuronal maturation of iN cells (Figure 3f). When iN cells were further cultured up to 16–18 d, cells in both the BAM and BAM/TES groups showed extensive neurite outgrowth (Figure 3g). On days 16–18, 31.3% and 61.2% Tuj1-positive iN cells in the BAM and BAM/TES groups, respectively, yielded positive results for MAP2 (Figure 3h). The average neurite length of iN cells in the BAM/TES group was longer than that of iN cells in the BAM group (0.10 µm for iN cells in the BAM group, and 0.17 mm for iN cells in the BAM/TES group; Figure 3i). On day 18 of reprogramming, neurite length of iN cells exposed to TES was as long as \approx 2.9 mm (Figure S4, Supporting Information). These results indicated

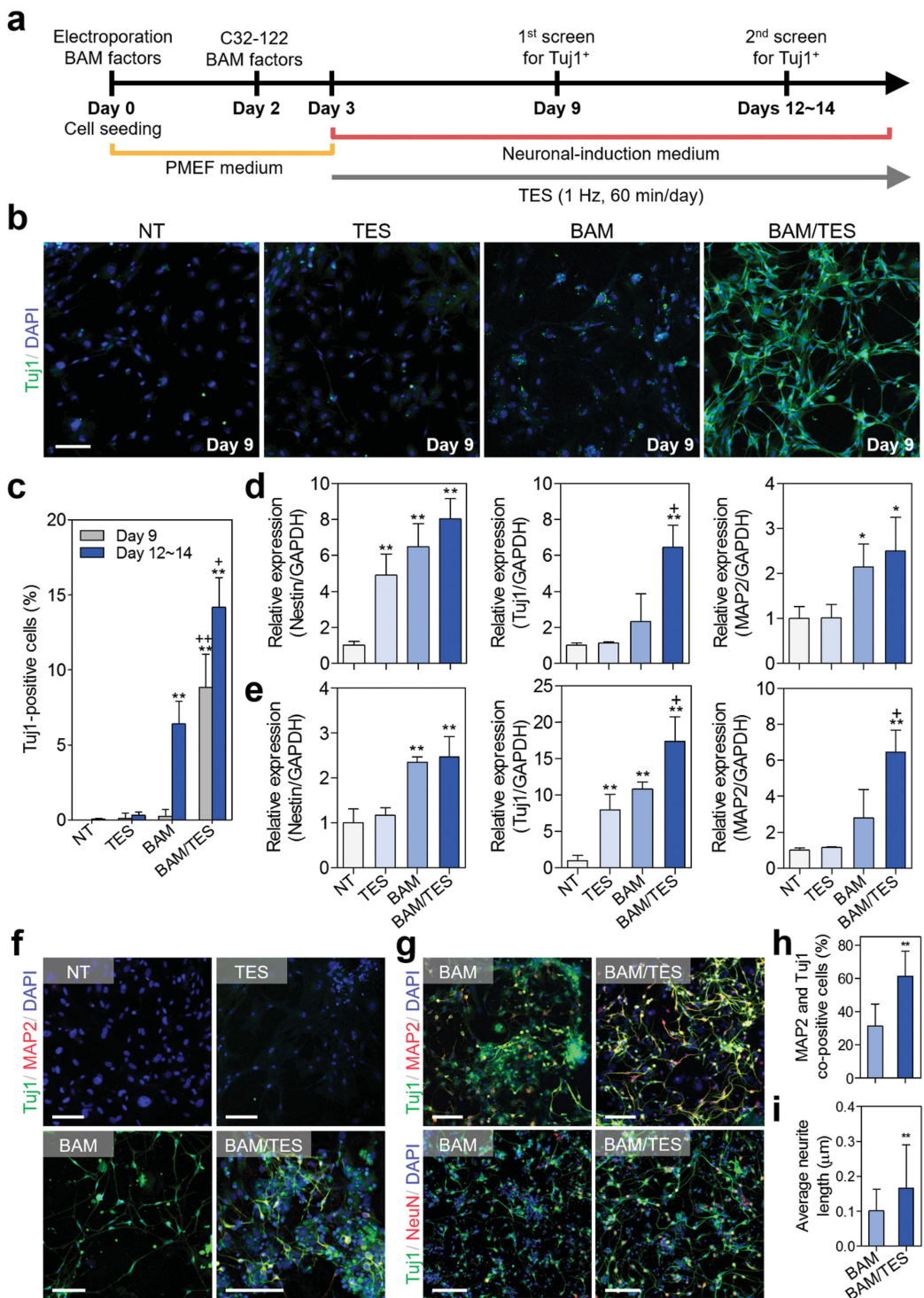


Figure 3. Accelerated conversion of PMEFs to neuronal cells and maturation of iN cells by using triboelectrical stimulation. a) Experimental outline of iN cell generation from PMEFs through nonviral delivery of genes encoding BAM TFs and exposure to TES. b) Expression of Tuj1 in cells in the NT, TES, BAM, and BAM/TES groups after 9 d of culture (scale bar = 100 μ m). c) Conversion efficiency for iN cell generation presented as the percentage ratio of Tuj1-positive cells to the initially seeded total cell population on days 9 and 12–14 (** P < 0.01 versus that in the NT group, $+P$ < 0.05 and ++ P < 0.01 versus that in the BAM group). d,e) Results of qRT-PCR for measuring the mRNA levels of neuronal-specific marker genes encoding nestin, Tuj1, and MAP2 on d) 6 and e) 12 d of culture (* P < 0.05 and ** P < 0.01 versus those in the NT group, $+P$ < 0.05 versus that in the BAM group). Immunofluorescence staining (Tuj1, MAP2, NeuN) of cells in the NT, TES, BAM, and BAM/TES groups on f) day 14 and of cells in the BAM and BAM/TES groups on g) days 16–18 in culture (scale bars = 100 μ m). Comparison of h) the percentage of MAP2-positive iN cells and i) average neurite length of iN cells in the BAM and BAM/TES groups on days 16–18 (** P < 0.01 versus that in the BAM group).

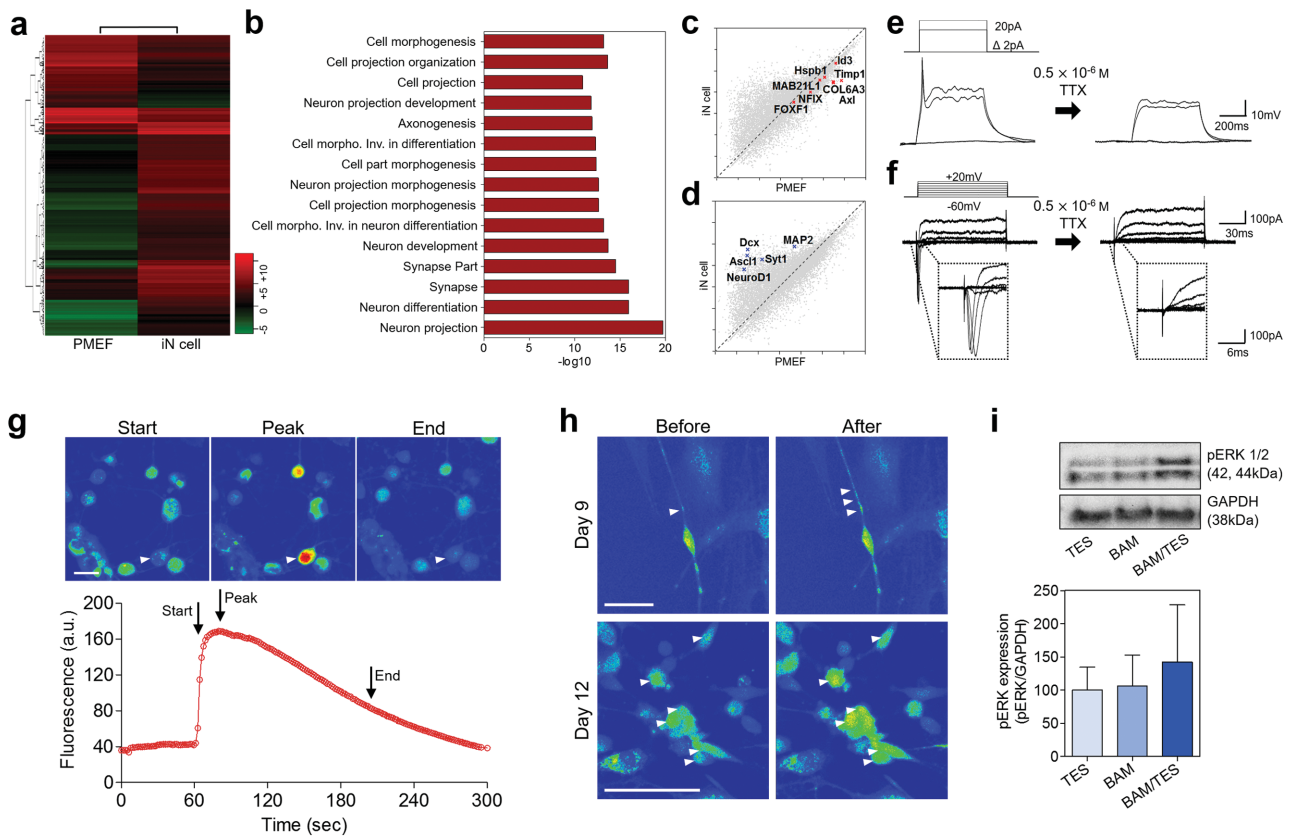


Figure 4. Global transcriptional profiles and electrophysiological functionalities of iN cells exposed to triboelectrical stimulation. a) Heat-map of genes differentially expressed during RNA-Seq analysis of PMEFs and iN cells transfected with BAM TF-expressing plasmids and exposed to TES. Expression values are represented in shades of red and green relative to being above (red) or below (green) the median expression value (log scale 2, from -5 to +10). b) Top 15 upregulated GO terms in iN cells compared with those in PMEFs. c,d) Scatter plots of gene expression changes showing (c) repression of fibroblast marker genes and (d) upregulation of neuronal marker genes in iN cells relative to that in PMEFs. e) Representative current-clamp recordings of action potentials recorded in iN cells exposed to TES at -60 mV in response to step depolarization by current injections. These action potential spikes disappeared after treatment with 0.5×10^{-6} M TTX. f) Representative traces of whole-cell Na^+ channel-mediated currents in iN cells exposed to TES in a voltage-clamp mode in the absence and presence of 0.5×10^{-6} M TTX. g) Cytosolic Ca^{2+} changes in iN cells on day 30 in response to treatment with 100×10^{-6} M glutamate (scale bar = 20 μm). h) Ca^{2+} imaging of Fluo-4 AM-treated iN cells during exposure to TES on days 9 and 12. White arrowheads indicate increase in fluorescence (scale bars = 50 μm). i) Representative western blotting images of phosphorylated ERK1/2 (pERK1/2) and housekeeping protein glyceraldehyde 3-phosphate dehydrogenase (GAPDH) in cells in the TES, BAM, and BAM/TES groups on day 7 (upper panel), and quantitative analysis of pERK1/2 expression relative to that of GAPDH in each group ($n = 3$, lower panel).

that TES exposure promoted the neuronal maturation of iN cells. After 21 d of culture, cells in both the BAM and BAM/TES groups showed distinctive neuronal morphologies, with extensive neurite growth (Figure S5a, Supporting Information). iN cells in BAM/TES group on day 30 showed punctate distribution of highly mature neuronal phenotype markers NeuN and synapsin I (SI), suggesting synaptic formation (Figure S5b Supporting Information). Moreover, iN cells exposed to TES yielded positive results for vesicular glutamate transporter 1 (vGlut1), a glutamatergic neuronal marker, and GAD67, a GABAergic neuronal marker (Figure S5b, Supporting Information), suggesting that these cells could further differentiate into excitatory or inhibitory neurons.

To assess whether iN cells derived from PMEFs that were nonvirally transfected with genes encoding neuronal TFs and exposed to TES showed global gene expression profiles specific to mature neurons, we investigated genome-wide transcriptional changes in iN cells reprogrammed for 30 d

by performing RNA sequencing (RNA-Seq; Figure 4a). We observed that iN cells showed significant changes in the expression of 859 genes (fold change, >2 ; $P < 0.05$) compared with PMEFs. Gene ontology (GO) analysis of genes upregulated in iN cells compared with those in PMEFs was conducted to confirm the shift in global transcriptional profiles to neuronal lineage. Notably, genes related to neuron development, differentiation, projection, and synapse were the top 5 GO terms upregulated in iN cells (Figure 4b). Fibroblast-related genes such as *Timp1*, *Id3*, *Axl*, *Hspb1*, *Nfix*, *Foxf1a*, *Snai*, and *Thy1* were repressed in iN cells (Figure 4c). In contrast, neuronal-related genes such as *Tuj1*, *Map2*, *Dcx*, *Ascl1*, and *NeuroD* and transcripts such as *Syp*, *Syt1*, and *Syn1* involved in synaptic formation were upregulated in iN cells (Figure 4d).

Whole-cell patch-clamp recordings were obtained to validate whether the functional activity of iN cells generated using TES was similar to that of mature neurons (Figure 4e,f). In the current-clamp mode, action potential could be elicited by

depolarizing the membrane (Figure 4e). In the voltage-clamp mode, fast-inactivating inward and outward currents, which corresponded to the opening of voltage-dependent Na^+ channels, were observed (Figure 4f). These results indicated that iN cells showed functional membrane properties and activities similar to those of normal neurons. Peaks corresponding to Na^+ current and action potential disappeared after treatment with tetrodotoxin (TTX), an Na^+ channel blocker (Figure 4e,f). Expression of functional ligand-gated channels in iN cells was examined by measuring intracellular changes in Ca^{2+} levels by using a Ca^{2+} -sensitive indicator Fluo-4 AM. Addition of neurotransmitter glutamate increased intracellular Ca^{2+} levels as indicated by an increase in the fluorescence of Fluo-4 AM-treated cells (Figure 4g; Video S1, Supporting Information), indicating that iN cells developed glutamate receptors during transdifferentiation. According to our RNA-Seq data, the expression of Ca^{2+} channels, K^+/Na^+ exchanger, and K^+ channels which are known to play important roles in electrophysiological functions is highly upregulated in iN cells compared to the PMEFs (Figure S6, Supporting Information). The expression of Ca^{2+} channels was highly upregulated in iN cells (*Cacna1b* by 3.73-fold, *Cacna1d* by 5.80-fold, *Cacna2d2* by 6.00-fold, *Cacna2d3* by 5.74-fold, *Cacng2* by 7.73-fold, and *Cacng4* by 7.78-fold), compared to the PMEFs (Figure S6a, Supporting Information). Several subtypes of Na^+/K^+ ATPase subunits were also highly expressed in iN cells (*Atp1a2* by 9.51-fold, *Atp1a3* by 8.92-fold, *Atp1b1* by 1.60-fold, *Atp1b2* by 7.73-fold, and *Atp2b3* by 7.23-fold) (Figure S6b, Supporting Information). The expression of K^+ leak channel subfamily K member 1, 2, and 3 (*KCNK1*, 2, 3) was increased with 5.08, 2.99, and 2.20-folds in iN cells, respectively, compared to the PMEFs (Figure S6c, Supporting Information). These results may indicate that the expression and activity of various ion channels and pumps important for electrophysiological functionality are highly upregulated in iN cells generated by TES.

Potential mechanisms underlying TES-induced accelerated transdifferentiation of PMEFs to iN cells were elucidated. Although the exact molecular mechanisms underlying the enhancement of neuronal differentiation after electrical stimulation are not well understood, some cellular responses induced by electrical stimulation have been identified.^[9,10c,11a] Electrical stimulation induces Ca^{2+} mobilization and protein kinase C activation as an early response through extracellular signal-regulated kinase 1/2 (ERK1/2)-dependent signaling pathways.^[9,11a,19] A study reported that electrical stimulation induced neuronal gene expression by activating N-type Ca^{2+} channels.^[20] To determine whether TES changed intracellular Ca^{2+} concentrations in iN cells, Fluo-4 AM-treated iN cells were observed under a confocal microscope during electrical stimulation. Results of confocal microscopy showed persistent increase in intracellular Ca^{2+} levels during exposure to TES on both days 9 and 12 (Figure 4h; Video S2 and S3, Supporting Information), suggesting that TES induced Ca^{2+} influx. This observation is significantly important because increased Ca^{2+} influx activates several important downstream cellular mechanisms, including neuronal extension, differentiation, and plasticity.^[20,21] ERK1/2 signalling pathway is suggested to be involved in neuronal differentiation after Ca^{2+} channel activation and Ca^{2+} influx.^[19] Our results showed an increase in the expression of phosphorylated

ERK1/2 on day 7 in cells transfected with BAM TF-expressing plasmids and exposed to TES (Figure 4i). Therefore, we inferred that TES induced Ca^{2+} channel activation, Ca^{2+} influx, and consequent ERK1/2 signal transduction that ultimately promoted the direct conversion of PMEFs to iN cells.

TES frequency may regulate iN cell conversion by altering voltage-gated Ca^{2+} channel expression. Fukui et al. previously reported that the expression of phosphorylated ERK in rat dorsal horn neuron was induced in a frequency-dependent manner during electrical stimulation.^[22] Zhao et al. reported that electrical stimulation increases c-fos expression via Ca^{2+} ion influx through both N-type and L-type calcium channels in rat superior cervical ganglion cells in a frequency-dependent manner.^[23] The increase in frequency resulted in enhanced expression of downstream gene, c-fos, and the increase in the number of c-fos-positive neurons was repressed by the treatment of inhibitors for both N-type and L-type calcium channels.^[23] Based on these previous reports, we can postulate that TES frequency would alter expression and activity of voltage-gated calcium channels, which affects iN cell conversion process.

To explore the feasibility of performing direct cell conversion *in vivo*, PBAE nanoparticles complexed with BAM TF-expressing plasmids were transfected into mouse dermal fibroblasts through an intradermal injection on days 0 and 2. On the day after the final injection, skin regions containing the transfected dermal fibroblasts were exposed to TES for 30 min per day for 14 d (Figure 5a). TES-generated electrical stimulation was applied to the skin by connecting the top and bottom plates of the TES to electrocardiogram patches attached to the skin in series at 2 cm intervals. The region of the skin injected with PBAE nanoparticles complexed with BAM TF-expressing plasmids was located between 2 electrocardiogram patches. Under periodic contact of 1 Hz frequency, the measured current from the skin was ≈ 80 nA (Figure 5b). To confirm direct cell conversion *in vivo*, skin tissue sections (Figure 5c–e; Video S4, Supporting Information) and whole skin tissues (Figure S7, Supporting Information) of treated mice were immunostained for Tuj1. The combination treatment with BAM TF-expressing plasmids and TES generated of Tuj1-positive cells, with an efficiency of 5.86% (Figure 5c). Most of these cells were present in the dermis and some were present in the epidermis (Figure 5e). Injection of BAM TF-expressing plasmids alone generated less number of Tuj1-positive cells, with an efficiency of 0.04% (Figure 5c,d). These data implied that TES enhanced the non-viral generation of Tuj1-positive iN cells from skin cells *in vivo*, suggesting its applicability in *in vivo* reprogramming.

Here, we show that nonviral delivery of genes encoding a set of neuronal TFs (BAM TFs) combined with electrical stimulation with a novel TES system rapidly and efficiently converted mouse fibroblasts into functional iN cells. To our knowledge, this is the highest efficiency of generating Tuj1-positive iN cells reported using a nonviral gene delivery method to date.^[8d,24] Transfection protocols used in this study involving transfection of BAM TF-expressing plasmids by performing electroporation and retransfection of the plasmids by using PBAE nanoparticles were optimized to increase the probability of transfecting PMEFs and newly divided cells over time with BAM TF-expressing plasmids. The efficiency of generating iN cells by transfecting BAM TF-expressing plasmids alone was

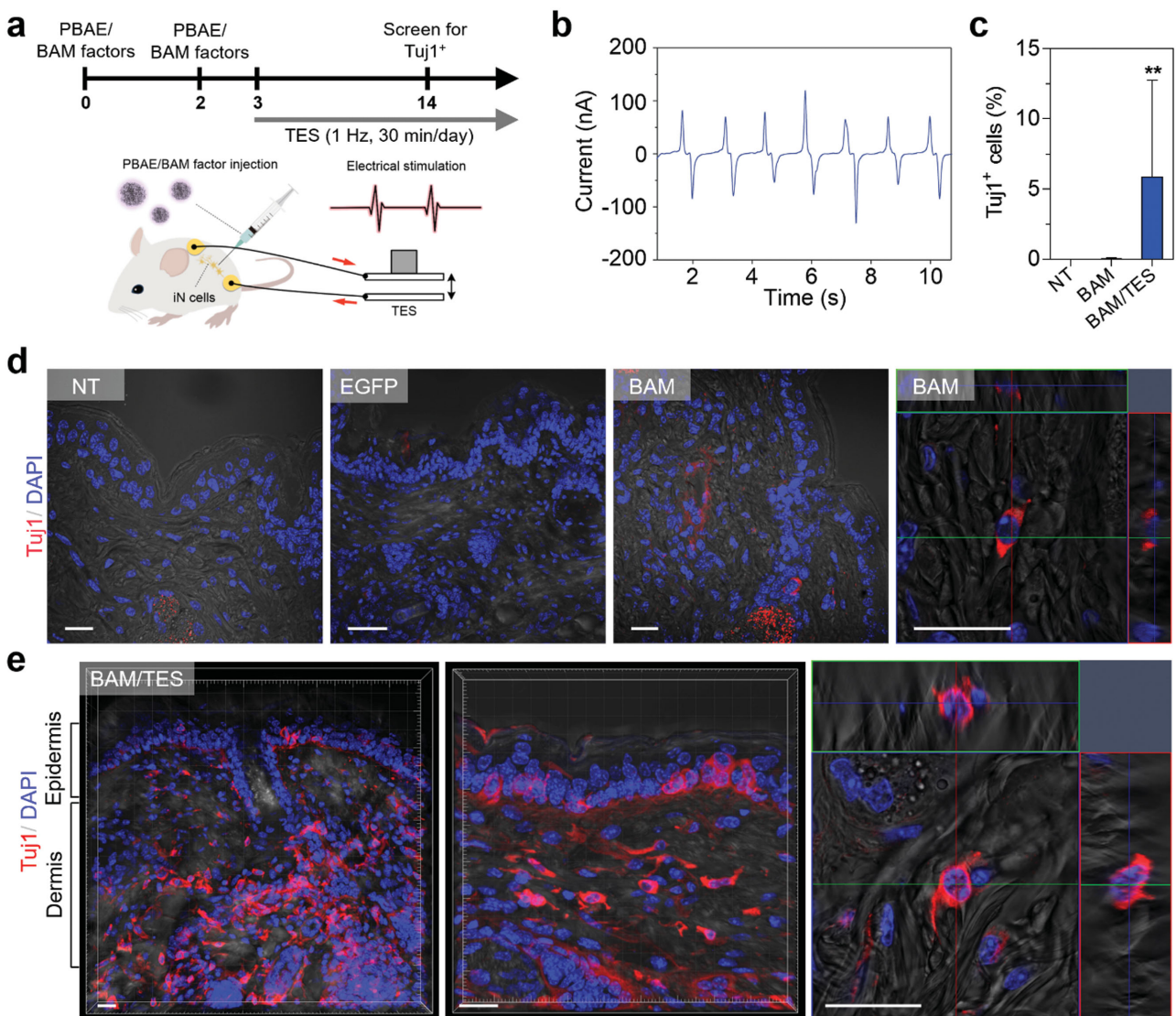


Figure 5. In vivo direct conversion of mouse dermal fibroblasts to iN cells. a) Schematic illustration and timeline of in vivo direct neuronal conversion. b) TES-generated electrical currents measured from the mouse skin, with 1 Hz pulse frequency. The currents were measured by connecting electrocardiogram patches in series with TES and by attaching them to the mouse skin. c) Quantification of Tuj1-positive cells generated by in vivo reprogramming of dermal fibroblasts of mice in the NT, BAM, and BAM/TES groups 14 d after injecting PBAE nanoparticles complexed with BAM TF-expressing plasmids (**P < 0.01 versus that in the BAM group). d,e) Immunostaining of skin tissue sections of (d) mice in the NT, enhanced green fluorescent protein (EGFP), and BAM groups and (e) mice in the BAM/TES group on day 14 by using anti-Tuj1 antibody (scale bars = 20 μ m).

6.41%. However, exposure to TES for a short duration after transfecting the BAM TF-expressing plasmids significantly decreased the conversion time to obtain Tuj1-positive iN cells by 3–5 d, increased iN cell generation efficiency to 14.17%, and enhanced neuronal maturation with increased neurite extension. Importantly, TES-generated iN cells showed various electrophysiological functionalities specific to mature primary neurons, including response to glutamate, Na⁺ currents, and action potential.

We also determined mechanisms underlying TES-induced accelerated conversion of PMEFs. Ca²⁺ live imaging showed changes in intracellular Ca²⁺ levels in reprogrammed cells after exposure to TES (Figure 4h). Ca²⁺ ions play a vital role in neuronal development and regulation.^[19,25] One of the

postulated mechanisms is that Ca²⁺ mobilization activated ERK1/2 signalling pathway and protein kinase C as an early response, resulting in the induction of genes involved in various cellular functions and cell maturation.^[9,10b,11b,19,26] We observed an increase in the phosphorylation of ERK1/2 on day 7 in cells transfected with BAM TF-expressing plasmids and exposed to TES (Figure 4i), suggesting that TES improved direct conversion to neuronal cells by inducing a series of cellular events, including Ca²⁺ channel activation, increased Ca²⁺ influx, and downstream ERK1/2 pathway activation.

We believe that use of the nonviral approach along with TES can be of significant therapeutic value for treating neurodegenerative diseases and neuronal disorders. The new approach of

using a triboelectric energy-harvesting system provides a less invasive or noninvasive, and nonchemical-based method for accelerating direct cell conversion and neuronal maturation. In addition, our study showed the possibility of achieving nonviral *in vivo* neuronal conversion by injecting PBAE nanoparticles complexed with BAM TF-expressing plasmids and by using a portable TES system. TES generates sustainable electrical signals from human motions for cell stimulation (Figure S8, Supporting Information). Therefore, for *in vivo* direct cell conversion, a TES could be developed as a cell replacement system in the context of electroceuticals.^[27] As a next step, we plan to develop a TES patch that can harvest energy from body motions such as breathing and cardiac pulses for direct cell conversion-based therapeutic application.

Experimental Section

Methods and any associated references are available in the Supporting Information.

Supporting Information

Supporting Information is available from the Wiley Online Library or from the author.

Acknowledgements

Y.J. and J.S. contributed equally to this work. This work was supported by grants (2012-0006689, 2013R1A1A2A10061422, and 2015R1A2A1A15053771) from the National Research Foundation of Korea (NRF) and a grant (HI13C1479) from the Korea Health Technology R&D Project funded by the Ministry of Health and Welfare, Republic of Korea. This work was also supported by the Mid-Career Researcher Program through an NRF grant funded by the MEST (2014R1A2A2A09053061), and the sensitivity touch platform development and new industrialization support program through the Ministry of Trade, Industry & Energy (MOTIE) and Korea Institute for Advancement of Technology (KIAT) (R0003423). Experimental protocols were approved by Yonsei University IACUC (IACUC-A-201507-348-01) in accordance with the guidelines of the National Institutes of Health Guide for the Care and Use of Laboratory Animals.

Received: April 9, 2016

Revised: May 14, 2016

Published online: June 15, 2016

- [1] a) J. Ladewig, P. Koch, O. Brüstle, *Nat. Rev. Mol. Cell Biol.* **2013**, *14*, 225; b) T. Vierbuchen, M. Wernig, *Nat. Biotechnol.* **2011**, *29*, 892.
- [2] a) M. B. Victor, M. Richner, T. O. Hermanstyne, J. L. Ransdell, C. Sobieski, P.-Y. Deng, V. A. Klyachko, J. M. Nerbonne, A. S. Yoo, *Neuron* **2014**, *84*, 311; b) A. S. Yoo, A. X. Sun, L. Li, A. Shcheglovitov, T. Portmann, Y. Li, C. Lee-Messer, R. E. Dolmetsch, R. W. Tsien, G. R. Crabtree, *Nature* **2011**, *476*, 228.
- [3] a) M. Caiazzo, M. T. Dell'Anno, E. Dvoretskova, D. Lazarevic, S. Taverna, D. Leo, T. D. Sotnikova, A. Menegon, P. Roncaglia, G. Colciago, *Nature* **2011**, *476*, 224; b) U. Pfisterer, A. Kirkeby, O. Torper, J. Wood, J. Nelander, A. Dufour, A. Björklund, O. Lindvall, J. Jakobsson, M. Parmar, *Proc. Natl. Acad. Sci. USA* **2011**, *108*, 10343.

- [4] M.-L. Liu, T. Zang, Y. Zou, J. C. Chang, J. R. Gibson, K. M. Huber, C.-L. Zhang, *Nat. Commun.* **2013**, *4*, 2183.
- [5] E. Y. Son, J. K. Ichida, B. J. Wainger, J. S. Toma, V. F. Rafuse, C. J. Woolf, K. Eggan, *Cell Stem Cell* **2011**, *9*, 205.
- [6] a) F. J. Najm, A. M. Lager, A. Zaremba, K. Wyatt, A. V. Caprariello, D. C. Factor, R. T. Karl, T. Maeda, R. H. Miller, P. J. Tesar, *Nat. Biotechnol.* **2013**, *31*, 426; b) Y. Xue, K. Ouyang, J. Huang, Y. Zhou, H. Ouyang, H. Li, G. Wang, Q. Wu, C. Wei, Y. Bi, *Cell* **2013**, *152*, 82.
- [7] M. Caiazzo, S. Giannelli, P. Valente, G. Lignani, A. Carissimo, A. Sessa, G. Colasante, R. Bartolomeo, L. Massimino, S. Ferroni, *Stem Cell Rep.* **2015**, *4*, 25.
- [8] a) C. E. Thomas, A. Ehrhardt, M. A. Kay, *Nat. Rev. Genet.* **2003**, *4*, 346; b) H. Yin, R. L. Kanasty, A. A. Eltoukhy, A. J. Vegas, J. R. Dorkin, D. G. Anderson, *Nat. Rev. Genet.* **2014**, *15*, 541; c) T. B. Lentz, S. J. Gray, R. J. Samulski, *Neurobiol. Dis.* **2012**, *48*, 179; d) A. F. Adler, C. L. Grigsby, K. Kulangara, H. Wang, R. Yasuda, K. W. Leong, *Mol. Ther.—Nucleic Acids* **2012**, *1*, e32.
- [9] Y.-J. Chang, C.-M. Hsu, C.-H. Lin, M. S.-C. Lu, L. Chen, *Biochim. Biophys. Acta* **2013**, *1830*, 4130.
- [10] a) J.-H. Lim, S. D. McCullen, J. A. Piedrahita, E. G. Loba, N. J. Olby, *Cell. Reprogram.* **2013**, *15*, 405; b) K.-A. Chang, J. W. Kim, J. A. Kim, S. Lee, S. Kim, W. H. Suh, H.-S. Kim, S. Kwon, S. J. Kim, Y.-H. Suh, *PloS One* **2011**, *6*, e18738; c) N. W. S. Kam, E. Jan, N. A. Kotov, *Nano Lett.* **2008**, *9*, 273.
- [11] a) N. A. McLean, B. F. Popescu, T. Gordon, D. W. Zochodne, V. M. Verge, *PLoS One* **2014**, *9*, e110174; b) A. A. Al-Majed, T. M. Brushart, T. Gordon, *Eur. J. Neurosci.* **2000**, *12*, 4381.
- [12] a) S. Xu, Y. Qin, C. Xu, Y. Wei, R. Yang, Z. L. Wang, *Nat. Nanotechnol.* **2010**, *5*, 366; b) C. Dagdeviren, S. W. Hwang, Y. Su, S. Kim, H. Cheng, O. Gur, R. Haney, F. G. Omenetto, Y. Huang, J. A. Rogers, *Small* **2013**, *9*, 3398; c) K. I. Park, C. K. Jeong, J. Ryu, G. T. Hwang, K. J. Lee, *Adv. Energy Mater.* **2013**, *3*, 1539; d) Z. L. Wang, J. Song, *Science* **2006**, *312*, 242; e) S. Wang, Z.-H. Lin, S. Niu, L. Lin, Y. Xie, K. C. Pradel, Z. L. Wang, *ACS Nano* **2013**, *7*, 11263; f) Z. L. Wang, *Adv. Mater.* **2012**, *24*, 280.
- [13] a) F.-R. Fan, Z.-Q. Tian, Z. Lin Wang, *Nano Energy* **2012**, *1*, 328; b) G. Zhu, Z.-H. Lin, Q. Jing, P. Bai, C. Pan, Y. Yang, Y. Zhou, Z. L. Wang, *Nano Lett.* **2013**, *13*, 847; c) S. Wang, L. Lin, Z. L. Wang, *Nano Lett.* **2012**, *12*, 6339; d) G. Zhu, J. Chen, Y. Liu, P. Bai, Y. S. Zhou, Q. Jing, C. Pan, Z. L. Wang, *Nano Lett.* **2013**, *13*, 2282; e) L. Lin, S. Wang, Y. Xie, Q. Jing, S. Niu, Y. Hu, Z. L. Wang, *Nano Lett.* **2013**, *13*, 2916; f) Z. Li, G. Zhu, R. Yang, A. C. Wang, Z. L. Wang, *Adv. Mater.* **2010**, *22*, 2534; g) J. Li, C. Zhang, L. Duan, L. M. Zhang, L. D. Wang, G. F. Dong, Z. L. Wang, *Adv. Mater.* **2016**, *28*, 106; h) X. Zhong, Y. Yang, X. Wang, Z. L. Wang, *Nano Energy* **2015**, *13*, 771; i) S. Niu, X. Wang, F. Yi, Y. S. Zhou, Z. L. Wang, *Nat. Commun.* **2015**, *6*, 8975.
- [14] Q. Zheng, B. Shi, F. Fan, X. Wang, L. Yan, W. Yuan, S. Wang, H. Liu, Z. Li, Z. L. Wang, *Adv. Mater.* **2014**, *26*, 5851.
- [15] W. Tang, J. Tian, Q. Zheng, L. Yan, J. Wang, Z. Li, Z. L. Wang, *ACS Nano* **2015**, *9*, 7867.
- [16] a) K. Y. Lee, J. Chun, J.-H. Lee, K. N. Kim, N.-R. Kang, J.-Y. Kim, M. H. Kim, K.-S. Shin, M. K. Gupta, J. M. Baik, S.-W. Kim, *Adv. Mater.* **2014**, *26*, 5037; b) L. Lin, Y. Xie, S. Wang, W. Wu, S. Niu, X. Wen, Z. L. Wang, *ACS Nano* **2013**, *7*, 8266.
- [17] a) F. Yang, S.-W. Cho, S. M. Son, S. R. Bogatyrev, D. Singh, J. J. Green, Y. Mei, S. Park, S. H. Bhang, B.-S. Kim, *Proc. Natl. Acad. Sci. USA* **2010**, *107*, 3317; b) S.-W. Cho, F. Yang, S. M. Son, H.-J. Park, J. J. Green, S. Bogatyrev, Y. Mei, S. Park, R. Langer, D. G. Anderson, *J. Controlled Release* **2012**, *160*, 515; c) H.-J. Park, J. Lee, M.-J. Kim, T. J. Kang, Y. Jeong, S. H. Um, S.-W. Cho, *Biomaterials* **2012**, *33*, 9148; d) J. Lee, I. Jun, H.-J. Park, T. J. Kang, H. Shin, S.-W. Cho, *Biomacromolecules* **2013**, *15*, 361.

- [18] K.-A. Chang, J. W. Kim, J. a. Kim, S. Lee, S. Kim, W. H. Suh, H.-S. Kim, S. Kwon, S. J. Kim, Y.-H. Suh, *PLoS One* **2011**, 6, e18738.
- [19] W. Wenjin, L. Wenchao, Z. Hao, L. Feng, W. Yan, S. Wodong, F. Xianqun, D. Wenlong, *Cell. Mol. Neurobiol.* **2011**, 31, 459.
- [20] T. A. Brosenitsch, D. M. Katz, *J. Neurosci.* **2001**, 21, 2571.
- [21] A. Ghosh, M. E. Greenberg, *Science* **1995**, 268, 239.
- [22] T. Fukui, Y. Dai, K. Iwata, H. Kamo, H. Yamanaka, K. Obata, K. Kobayashi, S. Wang, X. Cui, S. Yoshiya, *Mol. Pain* **2007**, 3, 1.
- [23] R. Zhao, L. Liu, A. R. Rittenhouse, *Eur. J. Neurosci.* **2007**, 25, 1127.
- [24] a) A. F. Adler, A. T. Speidel, N. Christoforou, K. Kolind, M. Foss, K. W. Leong, *Biomaterials* **2011**, 32, 3611; b) C. Maucksch, E. Firmin, C. Butler-Munro, J. Montgomery, M. Dottori, B. Connor, *J. Stem Cells Regen. Med.* **2012**, 8, 162.
- [25] a) N. C. Spitzer, *Nature* **2006**, 444, 707; b) S. S. Rosenberg, N. C. Spitzer, *Cold Spring Harb. Perspect. Biol.* **2011**, 3, a004259.
- [26] M. Yamada, K. Tanemura, S. Okada, A. Iwanami, M. Nakamura, H. Mizuno, M. Ozawa, R. Ohshima-Goto, N. Kitamura, M. Kawano, *Stem Cells* **2007**, 25, 562.
- [27] K. Famm, B. Litt, K. J. Tracey, E. S. Boyden, M. Slaoui, *Nature* **2013**, 496, 159.